Domain wall dynamics of ferrimagnets influenced by spin current near the angular momentum compensation temperature

V. V. Yurlov,[1] K. A. Zvezdin,[2,3,*] P. N. Skirdkov,[2,3] and A. K. Zvezdin[2]

[1]*Moscow Institute of Physics and Technology, Institutskiy Pereulok 9, 141700 Dolgoprudny, Russia*

[2]*Prokhorov General Physics Institute of the Russian Academy of Sciences, Vavilova 38, 119991 Moscow, Russia*

[3]*New Spintronic Technologies, Russian Quantum Center, Bolshoy Bulvar 30, Building 1, 121205 Moscow, Russia*

(Received 22 October 2020; revised 4 February 2021; accepted 13 April 2021; published 29 April 2021)

We report on a theoretical study of the spin current excited dynamics of domain walls (DWs) in ferrimagnets in the vicinity of the angular momentum compensation point. For a two-sublattice ferrimagnet effective Lagrangian and nonlinear dynamic equations are derived taking into account both the spin torques and the external magnetic field. The dynamics of the DW is calculated before and after the Walker breakdown for any direction of the spin current polarization. It is shown that for the in-plane polarization of the spin current, the DW mobility reaches a maximum near the temperature of the angular momentum compensation. On the contrary, for the out-of-plane spin polarization, the spin current with densities below the Walker breakdown does not excite DW dynamics. After overcoming the Walker breakdown, the domain wall velocity increases linearly with increasing current density. In this configuration of spin current polarization, the possibility of a gigahertz oscillation dynamics of the quasiantiferromagnetic vector under the action of a dampinglike torque at the angular momentum compensation point is demonstrated. Possible structures for experimental demonstration of the considered effects are discussed.

DOI: 10.1103/PhysRevB.103.134442

I. INTRODUCTION

Spintronics, which is a rapidly developing branch of nanoelectronics, is based on the concept that the principal role in information processing belongs to electron spins, not charges [1,2]. The mainstream of spintronics concentrates on the winning combination of the spin transport efficiency and nanoscale size of spintronic devices. In this regard, magnetic domain walls (DWs) have attracted increasing attention [3–5]: they can be used to store and transmit information in race track or magnetic random access memory devices [6–10].

Conventional spintronic devices use ferromagnetic (FM) materials due to their property of creating and subsequently exploiting the spin polarization of the conducting electrons. The natural limitations of ferromagnetic spintronic devices are associated with limited operating frequencies and overall energy efficiency. Recent advances in the field of spin current injection into insulating antiferromagnets (AFMs) revealed the prospects of antiferromagnetic spintronics, whose advantage is an extremely high frequency compared to the operating frequency of ferromagnetic devices [11,12]. At the same time antiferromagnetic spintronics has its own drawbacks associated with the difficulties in detecting the magnetization states and magnetization dynamics. These drawbacks motivate the accelerated development of ferrimagnetic spintronics, which combines ultrahigh operation frequencies close to those of antiferromagnetic devices with much more reliable ways to detect magnetization states. In these materials, a very rich and interesting in terms of fundamental and applied physics magnetization dynamics [13,14] is observed near the points of compensation of magnetization and angular momentum. Moreover, by manipulating the temperature of the ferrimagnet near the compensation points one can obtain outstanding magnetization switching characteristics [15–17]. It was shown that electric current can be an effective method for magnetization switching [18–21]. The GdFeCo ferrimagnetic layer demonstrates ultrafast magnetization reversal under the influence of femtosecond laser pulses in various experiments [22]. These results suggest that the ferrimagnetic-based structures can make a promising technological platform for ultrafast spintronic memory devices.

The angular momentum compensation point T_A, where $M_1/\gamma_1 = M_2/\gamma_2$, with γ_i being the gyromagnetic ratio of the ith sublattice ($i = 1, 2$), represents a very promising line of research of ferrimagnet (FiM) magnetization dynamics [13,23,24]. Recent field-driven experiments demonstrated high velocity and great mobility of a domain wall in FiM near T_A [25]. The next natural step in this direction is to use the spin currents to manipulate DW position and dynamics [26]. While the spin current induced phenomenon in ferromagnets seems to be very comprehensible, the mechanisms of spin transfer in AFMs and compensated FiMs have still not been figured out properly.

In the present research we develop a model to describe DW motion in ferrimagnets near the angular momentum compensation point in the case of arbitrary spin current polarization and torque type. DW dynamics influenced by a spin current in FiMs is studied generally by using the collective coordinates model and Landau-Lifshitz-Gilbert equation with the addition of spin-transfer torque components [27–29]. Here, instead, we employ the Lagrangian formalism for two sublattice

*zvezdin.ka@phystech.edu

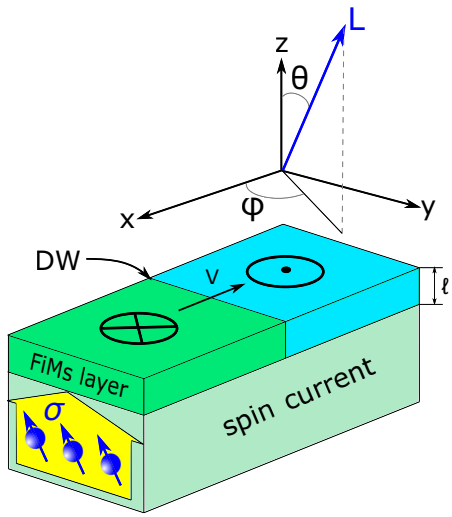

FIG. 1. Schematic of the considered FiMs with a single domain wall; $\boldsymbol{\sigma}$ is the polarization vector of the spin current, l is thickness of the sample, and θ and φ are the polar and azimuthal angles of the quasiantiferromagnetic vector $\mathbf{L}$.

ferrimagnets [30]. This approach allows us to strictly define ferrimagnetic parameters such as the width of the DW, velocity of the magnons, transverse magnetic susceptibility, effective Gilbert damping parameter, and gyromagnetic ratio by using perturbation theory.

We derive nonlinear dynamic equations based on the Lagrangian formalism, which is similar to Slonczewski equations [31]. Using this model, we calculate the dynamics of the domain wall in FiMs, depending on the direction of the polarizer, electric current density, and temperature, before and after the Walker breakdown. In our modeling we observe that for the in-plane polarization of the spin current, the DW mobility reaches a maximum near the temperature of the angular momentum compensation and vanishes after bypassing the Walker breakdown. For the out-of-plane spin polarization, in contrast, a spin current with the densities below the Walker breakdown does not excite the stationary dynamics of the DW. After overcoming the Walker breakdown, the domain wall velocity increases linearly with increasing electric current density. In this configuration of the spin current, near the compensation point T_A we observe gigahertz oscillations of the quasiantiferromagnetic vector.

II. MODEL AND BASIC EQUATIONS

We develop a model based on the Lagrange formalism for describing DW dynamics due to spin current. For two sublatticed FiMs ordering parameters related to magnetizations $\mathbf{M}_1$ and $\mathbf{M}_2$ of these sublattices can be introduced in the vicinity of compensation temperatures as quasiantiferromagnetic vector $\mathbf{L} = \mathbf{M}_1 - \mathbf{M}_2$ and ferromagnetic $\mathbf{M} = \mathbf{M}_1 + \mathbf{M}_2$ order parameters. We consider a spin current with a polarization $\boldsymbol{\sigma}$ flowing through the FiM film (see Fig. 1). The spin current excites a spin transfer torque acting on local magnetization of the ith sublattice and in the general case is composed of the in-plane and out-of-plane components $\mathbf{T}^i_{ST} = \mathbf{T}^i_{FL} + \mathbf{T}^i_{DL}$. The $\mathbf{T}^i_{FL}$ component due to its symmetry is usually referred to as a fieldlike torque and has the following form: $\mathbf{T}^i_{FL} \sim [\mathbf{M}_i \times \boldsymbol{\sigma}]$. The $\mathbf{T}^i_{DL}$ torque component has a symmetry similar to the damping torque and is usually referred to as a dampinglike torque (or an antidampinglike torque): $\mathbf{T}^i_{DL} \sim [\mathbf{M}_i \times [\mathbf{M}_i \times \boldsymbol{\sigma}]]$. Typically, the magnitude of the antidampinglike torque component is significantly larger than the fieldlike one for magnetic tunnel junctions; however, in the case of spin-orbit torques they can be of a similar magnitude.

The magnetization dynamics is described by a system of Euler-Lagrange equations:

$$\begin{aligned}\frac{d}{dt}\left(\frac{\partial \mathcal{L}}{\partial \dot{\theta}_i}\right) - \frac{\delta \mathcal{L}}{\delta \theta_i} &= -\frac{\partial \mathcal{R}_i}{\partial \dot{\theta}_i} - \frac{\partial W}{\partial \dot{\theta}_i},\\ \frac{d}{dt}\left(\frac{\partial \mathcal{L}}{\partial \dot{\varphi}_i}\right) - \frac{\delta \mathcal{L}}{\delta \varphi_i} &= -\frac{\partial \mathcal{R}_i}{\partial \dot{\varphi}_i} - \frac{\partial W}{\partial \dot{\varphi}_i},\end{aligned} \tag{1}$$

where $\mathcal{L}$ and $\mathcal{R}_i$ are the Lagrangian and Rayleigh functions, W is spin transfer torque power density, and θ_i and φ_i are the polar and azimuthal angles characterizing the orientation of the ith sublattice magnetization ($i = 1, 2$). Note that δW represents the external spin current effect on the magnetic structure and consists of the dampinglike and fieldlike components. Due to its symmetry the fieldlike component can be included in the Lagrangian by using the quasiantiferromagnetic approximation. Thus, δW in the Euler-Lagrange equations consist of only the dampinglike spin current component. Hereafter we turn to the effective Lagrangian $\mathcal{L}_{\text{eff}}$, effective Rayleigh function $\mathcal{R}_{\text{eff}}$, and power density of a spin current δW in the quasiantiferromagnetic approximation applicable in the vicinity of compensation temperatures (see [32] for a derivation of the effective Lagrangian) [30]. The procedure to get these equations is quite similar to the approach that was used in [33] to study DW dynamics in antiferromagnets and compensated ferrimagnets:

$$\begin{aligned}\mathcal{L}_{\text{eff}} &= \frac{\chi_\perp}{2}\left(\frac{\dot{\theta}}{\overline{\gamma}_{\text{eff}}}\right)^2 + m\left(H - \frac{\dot{\varphi}}{\gamma_{\text{eff}}}\right)\cos\theta\\ &\quad + \frac{\chi_\perp}{2}\left(H - \frac{\dot{\varphi}}{\overline{\gamma}_{\text{eff}}}\right)^2 \sin^2\theta - K_u \sin^2\theta\\ &\quad - K_\perp \sin^2\theta\sin^2\varphi - A\left[\left(\frac{d\theta}{dx}\right)^2 + \sin^2\theta\left(\frac{d\varphi}{dx}\right)^2\right]\\ &\quad - \frac{\chi_\perp}{2}\left(\frac{\overline{B}}{\mathcal{M}}\right)^2 [\sin^2\theta n_\perp + \cos^2\theta\cos^2(\varphi - \psi)n_\parallel\\ &\qquad + \sin^2(\varphi - \psi)n_\parallel],\\ R_{\text{eff}} &= \frac{\alpha_{\text{eff}}\mathcal{M}}{\gamma_{\text{eff}}}(\dot{\theta}^2 + \sin^2\theta\dot{\varphi}^2),\\ \delta W &= -\overline{A}\sin(\varphi - \psi)n_\parallel\delta\dot{\theta}\\ &\quad + [-\overline{A}n_\perp\sin^2\theta + \overline{A}n_\parallel\cos\theta\cos(\varphi - \theta)]\delta\dot{\varphi},\end{aligned} \tag{2}$$

where $m = M_2 - M_1$, $\mathcal{M} = M_1 + M_2$, $\chi_\perp = \mathcal{M}/H_{ex}$ is the transverse magnetic susceptibility, and H_{ex} is an exchange magnetic field acting between sublattices. K_u and $K_\perp$ are constants of uniaxial and in-plane magnetic anisotropies, respectively. A is an exchange stiffness constant. θ and φ are the polar and azimuthal

angles of a quasiantiferromagnetic vector $\mathbf{L}$, $\mathbf{H} = (0, 0, H_z)$ is a magnetic field applied along the "easy magnetization axis." $\alpha_{\text{eff}} = \overline{\alpha} m/(m - m_0)$, $\gamma_{\text{eff}} = \overline{\gamma} m/(m - m_0)$, $\overline{\gamma}_{\text{eff}} = \overline{\gamma}(1 - m m_0/\mathcal{M}^2)^{-1}$, $\overline{\alpha} = (\alpha_1\gamma_2 + \alpha_2\gamma_1)/2(\gamma_1 + \gamma_2)$, and $1/\overline{\gamma} = (1/\gamma_1 + 1/\gamma_2)/2$, where α_i and γ_i are the damping constant and gyromagnetic ratio for the ith sublattice, respectively, and $m_0 = \mathcal{M}(\gamma_1 - \gamma_2)/(\gamma_1 + \gamma_2)$. $\overline{A} = \hbar J P_{DL}/(2el)$ and $\overline{B} = \hbar J P_{FL}/(2el)$ are the damping (or antidamping) and fieldlike spin transfer torque coefficients, where J is the electrical current density, l is the thickness of the magnetic film, and $e > 0$ is the electron charge. $n_\perp$ and $n_\parallel$ are the out-of- and in-plane components of unit vector $\mathbf{n} = (n_x, n_y, n_z)$ along the polarization of spin current $\boldsymbol{\sigma}$, and ψ is an angle between the projection of the polarization vector of the spin current $\boldsymbol{\sigma}$ on the x-y plane and the x axis. P_{DL} and P_{FL} are the damping (or antidamping) and fieldlike polarizations of the spin current, respectively.

Implementing the procedure described in the Supplemental Material, we derive the system of dynamic equations for the 180° DW without external magnetic field:

$$\frac{2\overline{\alpha}\mathcal{M}}{\overline{\gamma}\Delta_0}\dot{q} + m\frac{\dot{\varphi}}{\gamma_{\text{eff}}} = \widetilde{T}_\theta,$$
$$-\frac{\chi_\perp}{\overline{\gamma}_{\text{eff}}^2}\ddot{\varphi} + \frac{m}{\gamma_{\text{eff}}}\frac{\dot{q}}{\Delta_0} - K_\perp \sin 2\varphi - \frac{2\overline{\alpha}\mathcal{M}}{\overline{\gamma}}\dot{\varphi} = \widetilde{T}_\varphi, \qquad (3)$$

where q is a coordinate of the DW center and $\Delta_0 = \sqrt{A/K_u}$ is the width of the DW. The spin transfer torque components are written as

$$\widetilde{T}_\theta = -\frac{\pi}{2}\overline{A}\sin(\varphi - \psi)n_\parallel,$$
$$\widetilde{T}_\varphi = -\overline{A}n_\perp + \frac{\chi_\perp}{2}\left(\frac{\overline{B}}{\mathcal{M}}\right)^2 \sin 2(\varphi - \psi)n_\parallel. \qquad (4)$$

Note that in the general case the width of the DW is determined as $\Delta = \Delta_0\sqrt{1 - (\dot{q}/c)^2}$, where $c = \overline{\gamma}_{\text{eff}}\sqrt{2A/\chi_\perp}$ is the magnon velocity (see [32] for Euler-Lagrange equations and the Fredholm alternative). For our set of parameters it can be estimated as $c \sim 8$ km/s. As a result, the variation of the DW width for the considered velocities is of the order of 1% ($\Delta/\Delta_0 \sim 0.01$). Thus, we can assume that $\dot{q} \ll c$ and DW width $\Delta \approx \Delta_0$.

III. DYNAMIC EQUATION ANALYSIS

To understand the peculiar features of the current induced DW dynamics in compensated FiMs following from Eqs. (3) and (4), we analyze several particular cases. To calculate the DW dynamics we use typical GdFeCo parameters [25]: $K_u \sim 1\times10^5$ erg/cm^3, $\mathcal{M} \approx 900$ emu/cm^3, $\overline{\alpha} \sim 0.02$, $\overline{\gamma} \sim 2\times10^7$, $A \sim 1\times10^{-6}$ erg/cm, $g_d = 2.2$, $g_f = 2$, $T_M = 220$ K, $T_A = 310$ K, and $l = 10$ nm, where g_d and g_f are Landé g factors for d and f sublattices, respectively. The constant of in-plane magnetic anisotropy in the case of an infinite film is $K_\perp = 2\pi\,\text{m}^2$; however, in the case of a narrow FiM nanowire it has a different form due to magnetostatic interaction. Note that all dynamic parameters (such as velocity, DW displacement, and others) are functions of $\nu = m/\mathcal{M}$, which can be rewritten in terms of temperature T by using the following expression:

$$\nu = \frac{m}{\mathcal{M}} = \frac{T - T_M}{T^*}, \qquad (5)$$

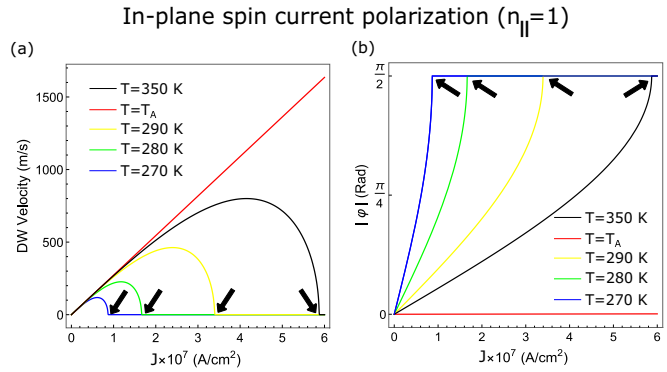

FIG. 2. (a) Average DW velocity in Walker and post-Walker regimes as a function of the electrical current density J. (b) Absolute value of the azimuthal angle φ in Walker and post-Walker regimes as a function of the electrical current density J. Blue, green, yellow, red, and black curves correspond to the temperatures $T = 270$ K, $T = 280$ K, $T = 290$ K, $T = T_A$, and $T = 350$ K respectively; the black arrows indicate the transition in the post-Walker regime. All curves are plotted for the in-plane spin current polarization.

where $T^* = 1891$ K is obtained from the GdFeCo parameters [25]. For all further mentioned modeling results $P_{DL} = 0.3$ and $P_{FL} = 0.03$.

First, let us analyze DW dynamics for the in-plane spin current when $K_\perp \neq 0$ and the spin polarization is along the y axis $n = (0, 1, 0)$ ($\psi = \pi/2$ and $n_\parallel = 1$). In this geometry stationary DW motion ($\dot{\varphi} = 0$ and a constant DW velocity) is observed below the Walker breakdown. In T_A the azimuthal angle φ tends to zero [see the red curve in Fig. 2(b)], and the stationary DW motion is observed with the velocity $\dot{q}/\Delta_0 = \pi\overline{\gamma}\overline{A}/4\overline{\alpha}\mathcal{M}$, which follows from the first equation in (3). As follows from (3) and (4) in this case the dampinglike (or antidampinglike) spin transfer torque component with magnitude $\overline{A}$ initiates DW dynamics, while the fieldlike one modifies only the magnetostatic term. The magnitude of the azimuthal angle φ increases with increasing electric current density and tends to $\pi/2$, which is demonstrated in Fig. 2(b). Note that in the case of the in-plane polarizer after reaching the critical current density corresponding to the Walker breakthrough $J^* = 16el|\alpha_{\text{eff}}|K_\perp/\pi\nu\hbar P_{AD}$, there is no domain wall motion observed; it is indicated by the black arrows in the Figs. 2(a) and 2(b). We can see that in the angular momentum compensation temperature $\alpha_{\text{eff}} \to +\infty$ and critical current density $J^* \to +\infty$. Therefore, in T_A stationary DW motion is observed without post-Walker range. This range (after Walker breakdown) corresponds to the constant azimuthal angle $\varphi \approx \pi/2$. Spin current cannot push the domain wall when the angle φ reaches $\pi/2$ [see Fig. 2(b)] for the case of in-plane polarization. This means that the steady precessional motion of the DW is impossible for in-plane polarized spin current, and the DW velocity eventually drops to zero for all temperatures except for T_A. A similar situation was observed for DW dynamics in a ferromagnetic system with perpendicular magnetic anisotropy [34], when DW dynamics after Walker breakdown vanished in the case of planar spin polarization.

Now let us discuss a more difficult situation in which $\boldsymbol{\sigma}$ is parallel to the z axis $\mathbf{n} = (0, 0, 1)$ and $n_\perp = 1$. Actually, if we

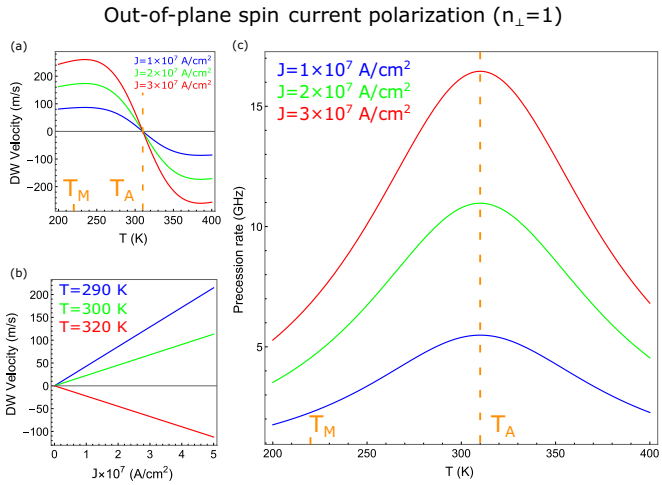

FIG. 3. (a) Dependence of the DW velocity on temperature at different current densities. (b) Dependence of the DW velocity on electrical current density at different temperatures. (c) Precession rate as a function of temperature at different current densities. All curves are plotted for the out-of-plane spin current polarization.

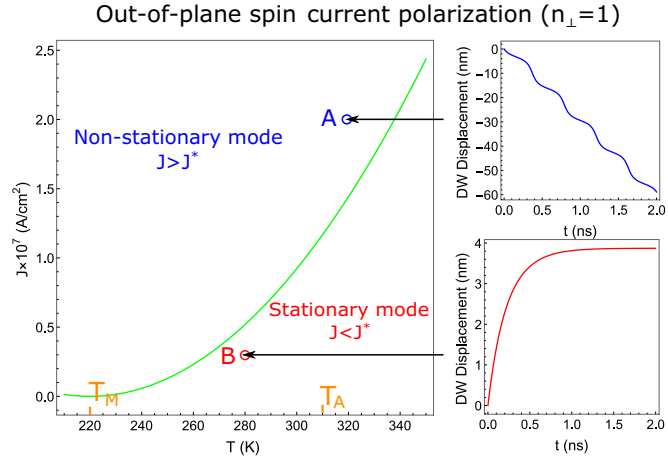

FIG. 4. J-T diagram which describes the ranges of steady and nonsteady motions of the DW. The green curve shows the temperature dependence of the critical current J^*; the ranges above ($J > J^*$) and below ($J < J^*$) the green curve correspond to nonstationary (post-Walker) and stationary (Walker) modes of the DW, respectively. Insets show the time dependence of DW displacement in the nonstationary range for point A ($T = 320$ K and $J = 2\times10^7$ A/cm^2) and the stationary range for point B ($T = 280$ K and $J = 0.3\times10^7$ A/cm^2) of the diagram. All curves are plotted for the out-of-plane spin current polarization.

assume that $K_\perp = 0$, $\chi_\perp \ll 1$ and consider the temperatures in the vicinity of the angular momentum compensation point T_A, the system (4) describes the steady motion of the DW with velocity $\dot{q}$ and precession rate $\dot{\varphi}$:

$$\frac{\dot{q}}{\Delta_0} = -\frac{\overline{\gamma}}{2\mathcal{M}\overline{\alpha}}\frac{\overline{A}\nu/2\alpha_{\text{eff}}}{1+(\nu/2\alpha_{\text{eff}})^2}, \tag{6}$$

$$\dot{\varphi} = \frac{\overline{\gamma}}{2\mathcal{M}\overline{\alpha}}\frac{\overline{A}}{1+(\nu/2\alpha_{\text{eff}})^2}. \tag{7}$$

By using Eq. (5) we can rewrite (6) and (7) in terms of temperature T and study the dependence of the DW velocity and precession rate on temperature and current density. Figure 3(a) demonstrates that the DW velocity has two maximum values near the angular momentum compensation point and these values increase with the growth in current density. These curves are asymmetric with respect to T_A. Thus, the velocity of the DW changes its sign passing through the angular momentum compensation point. This situation is also realized in Fig. 3(b), where the dependence of the DW velocity on electric current density at different temperatures is given. As seen from Eq. (6) DW velocity linearly depends on the electrical current density. The blue and green lines [see Fig. 3(b)] lie below T_A, and the slopes of these curves (DW mobility $\dot{q}/J$) decrease. The DW velocity changes direction above the angular momentum compensation point [red curve in Fig. 3(b)].

Note that the DW velocity reaches 260 m/s at current densities of about 3×10^7 A/cm^2. The precession rate is not zero $\dot{\varphi} \neq 0$ in the vicinity of the angular momentum compensation temperature compared with field-driving DW motion [35] (where magnetic field is applied along the easy magnetization axis). Equation (7) shows that $\dot{\varphi}$ reaches its maximum by about 17 GHz at low current density ($\sim3\times10^7$ A/cm^2) near T_A [see in Fig. 3(c)]. Following from Eqs. (6) and (7), in the case of the considered polarization direction both the oscillation of the φ angle and DW motion are triggered by the damping (or antidamping) spin transfer torque component with magnitude $\overline{A}$; hence, the DW dynamic and oscillation freeze without spin current. The fieldlike spin transfer torque is neglected in the out-of-plane spin current polarization case due to decomposition of the Lagrangian of the two-sublattice ferrimagnet as a next-order small parameter (see [32] for the spin transfer torque power density in a ferrimagnet).

Let us analyze the DW dynamic in the presence of in-plane magnetic anisotropy $K_\perp \neq 0$ and $\mathbf{n} = (0, 0, 1)$. We find out that there are two different regimes of the DW motion: steady ($\dot{\varphi} = 0$) and nonsteady ($\dot{\varphi} \neq 0$). Let us discuss the nonsteady one. An analytical solution to the system of differential equations (4) can be written as

$$\tan\varphi = \frac{J^*}{J} + \sqrt{\left[1-\left(\frac{J^*}{J}\right)^2\right]}\tan(\omega_0 t + \varphi_0), \tag{8}$$

where $J^* = \frac{4\pi\mathcal{M}^2\nu^2 el}{\hbar P_{DL}}$ is the critical current density, $\omega_0 = \frac{\overline{\gamma}}{\overline{\alpha}}\frac{\pi\nu^2\mathcal{M}\sqrt{1-(J^*/J)^2}}{1+(\nu/2\alpha_{\text{eff}})^2}$, $\varphi_0 = \arctan\frac{J^*/J}{\sqrt{1-(J^*/J)^2}}$. The nonstationary regime is realized when the current density J is higher than the critical current J^* ($J > J^*$). This situation is represented by the J-T diagram in Fig. 4, where the green curve is the temperature dependence of the critical current density J^*. Equation (8) describes the oscillation of the angle φ in the nonstationary range of the J-T diagram ($J > J^*$), and the inset for point A in Fig. 4 shows the time dependence of the DW displacement in this range at fixed temperature $T = 320$ K and current density $J = 2\times10^7$ A/cm^2. The stationary regime of the DW is realized when the current density J is lower than the critical current J^*. The inset in Fig. 4 for point B ($T = 280$ K and $J = 0.3\times10^7$ A/cm^2) shows that after a small period of

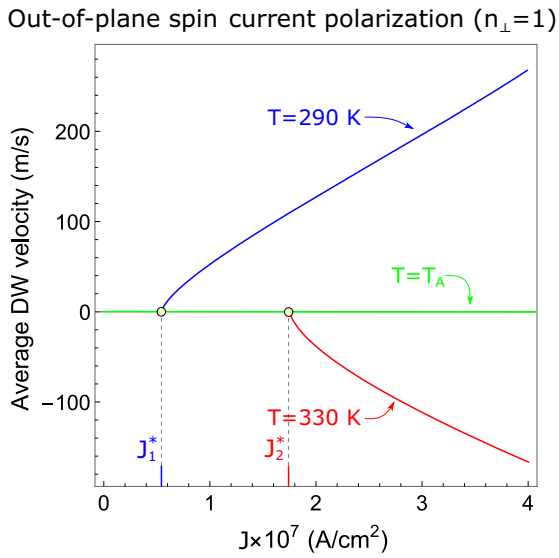

FIG. 5. Average DW velocity in the stationary and nonstationary modes as a function of the electrical current density J. Blue, green, and red curves correspond to temperatures $T = 290$ K, $T = T_A$, and $T = 330$ K, respectively; $J^*_{1,2}$ are critical current densities which correspond to $T = 290$ K and $T = 330$ K, respectively. All curves are plotted for the out-of-plane spin current polarization.

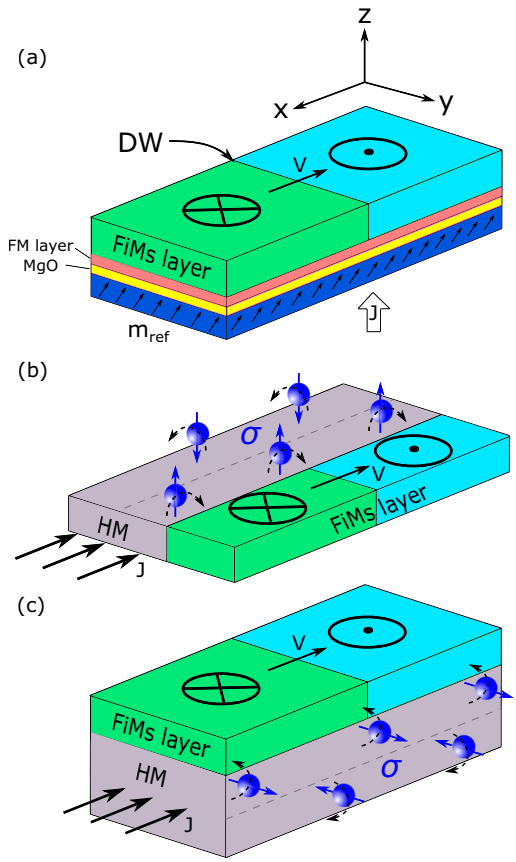

FIG. 6. Examples of (a) the MTJ base and (b) and (c) spin Hall based structures, which can be used to observe reported DW motion and oscillation regimes in a FIM film or nanostripe. (b) corresponds to the perpendicular direction of spin current polarization $\boldsymbol{\sigma}$, and (c) corresponds to the planar direction.

time, ∼0.15 ns, the DW displacement stops changing in time. Therefore, the precession rate $\dot{\varphi} = 0$, the velocity of the DW tends to zero, and the magnetization freezes in the stable state, which corresponds to the equation $\sin 2\varphi = J/J^*$ following (3). Hence, the stationary (Walker) mode in the considered case corresponds to the absence of DW motion, while the nonstationary mode is responsible for DW motion.

The dependence of the average DW velocity on the electrical current density in the stationary and nonstationary regimes is shown in Fig. 5. In the stationary mode the DW velocity is zero. Near the critical current J^* an increase in the value of velocity occurs. However, in the nonstationary mode ($J > J^*$) the average DW velocity linearly increases. Note that in the angular momentum compensation point the average velocity is equal to zero (green curve in Fig. 5). In addition Fig. 5 shows that velocity changes sign when passing through T_A, which is demonstrated by the blue ($T = 280$ K $< T_A$) and red ($T = 330$ K $< T_A$) curves in Fig. 5. These results are consistent with the J-T diagram in Fig. 4. It is important to note that in the nonstationary mode nonlinear spin waves can be excited and affect the dynamics of the DW. However, frequencies of the spin wave in ferrimagnetic or antiferromagnetic materials lie in the terahertz range [27,36,37]. In contrast the precession rate of the quasiantiferromagnetic vector lies in the gigahertz range, and we suppose that nonlinear spin waves have a weak effect on the DW dynamics. Moreover, our model itself has a limitation (see [32] for limits of the applicability of the presented model) in the precession rate which coincides with the frequencies of spin waves.

Now, let us discuss the directions of the spin current polarization $\boldsymbol{\sigma}$ and type of torques, which can lead to the effects mentioned above, and the possibility of their experimental realization. Following the reported results, the damping (or antidamping) spin transfer torque is responsible for the considered motion and oscillation regimes for both planar and perpendicular spin current polarizations $\boldsymbol{\sigma}$.

The first possible way to create a damping (or antidamping) torque is to use the magnetic tunnel junction (MTJ) structure. It consists of a free magnetic layer and a polarizer, which are separated by a thin insulating material (usually MgO). In such a structure electric current flows perpendicularly to the plane and creates Slonczewski torque in the free layer, while the spin current polarization $\boldsymbol{\sigma}$ direction is determined by the magnetization direction of the polarizer. An example of the MTJ structure is presented in Fig. 6(a). The typical polarization value P_{DL} in the MTJ with ferromagnets is about 0.2–0.4. Hence, one can add a thin FM layer between MgO and FIMs, which is usually done even in the classic MTJ to improve Tunnel magnetoresistance and polarization values [10] to achieve the level of $P_{DL} = 0.3$ used in our simulations.

Another way to create a damping (or antidamping) torque is to use a heavy metal/FIM heterostructure. In such a structure electric current flows through a heavy metal (like Ta, W, Pt, Au, etc.) in the film plane, and due to the spin Hall effect it creates a perpendicular spin current with polarization $\boldsymbol{\sigma}$, which is perpendicular to both electric and spin currents. This spin current can create an antidamping torque in the FIM.

Examples of spin Hall geometry in the case of perpendicular and planar polarizations $\boldsymbol{\sigma}$ are shown in Figs. 6(b) and 6(c), respectively. The value of polarization in these cases is equal to the spin Hall angle. This angle can be as high as 0.3 [38,39], which again makes our $P_{DL} = 0.3$ reasonable. Moreover, it is possible to use a topological insulator instead of a heavy metal to achieve spin Hall angles greater than 1 [40], which significantly reduces the required current density.

IV. DISCUSSION AND CONCLUSION

A theoretical study of the DW dynamics caused by the spin current near the angular momentum compensation point was carried out using the Lagrangian formalism. The nonlinear dynamic equations describing the DW motion are derived from the effective Lagrangian of two sublattice ferrimagnets. We analyze the DW motion for different directions of the spin current polarizations and show different types of magnetic heterostructures for which such a spin current polarization can be realized. In the case of an out-of-plane polarizer $[n = (0, 0, 1)]$ we analyzed the dependence of DW velocity and precession rate on temperature and current density. We foresee the possibility of generating oscillations of the quasiantiferromagnetic vector $\mathbf{L}$ with frequencies of about 17 GHz at low current densities in the vicinity of the angular momentum compensation temperature. These oscillations are initiated by the spin-transfer torque. Precessional motion may be associated with a recent micromagnetic modeling of terahertz oscillation caused by spin current in antiferromagnetic materials [41] at high current densities. Furthermore, the DW velocity changes direction when passing through this temperature, and this effect is observed experimentally in the GdFeCo ferrimagnet due to the spin current [42]. We explored the DW motion in the stationary (Walker) and nonstationary (post-Walker) modes and constructed a diagram that provides the values of current densities and temperatures for which these modes are realized. The model showed that in the Walker regime no DW motion occurs, while in the post-Walker range DW velocity increases linearly with the current. Note that a similar dependence of the DW velocity was observed due to the spin Hall effect [26] in the TbCo ferrimagnet sample in the presence of an external magnetic field. We also analyzed the DW dynamics for the in-plane spin current polarization and obtained the dependence of the DW velocity on the current in the Walker and post-Walker modes. Finally, we determined the directions of the spin current polarization $\boldsymbol{\sigma}$ and the types of torques which lead to the above effects and the possibility of their experimental implementation. These results can be useful for the experimental study of domain wall dynamics in ferrimagnets.

ACKNOWLEDGMENT

This research was supported by RSF Grant No. 19-12-00432.

[1] M. Tsoi, R. E. Fontana, and S. S. P. Parkin, Appl. Phys. Lett. **83**, 2617 (2003).
[2] J. Grollier, P. Boulenc, V. Cros, A. Hamzić, A. Vaurés, A. Fert, and G. Faini, Appl. Phys. Lett. **83**, 509 (2003).
[3] G. S. D. Beach, C. Nistor, C. Knutson, M. Tsoi, and J. L. Erskine, Nat. Mater. **4**, 741 (2005).
[4] Z. Li and S. Zhang, Phys. Rev. B **70**, 024417 (2004).
[5] J. Münchenberger, G. Reiss, and A. Thomas, J. Appl. Phys. **111**, 07D303 (2012).
[6] S. S. P. Parkin, M. Hayashi, and L. Thomas, Science **320**, 190 (2008).
[7] A. Shadman and J.-G. J. Zhu, Appl. Phys. Lett. **114**, 022403 (2019).
[8] A. V. Khvalkovskiy, K. A. Zvezdin, Y. V. Gorbunov, V. Cros, J. Grollier, A. Fert, and A. K. Zvezdin, Phys. Rev. Lett. **102**, 067206 (2009).
[9] P. N. Skirdkov, K. A. Zvezdin, A. D. Belanovsky, J. Grollier, V. Cros, C. A. Ross, and A. K. Zvezdin, Appl. Phys. Lett. **104**, 242401 (2014).
[10] A. Chanthbouala, R. Matsumoto, J. Grollier, V. Cros, A. Anane, A. Fert, A. V. Khvalkovskiy, K. A. Zvezdin, K. Nishimura, Y. Nagamine, H. Maehara, K. Tsunekawa, A. Fukushima, and S. Yuasa, Nat. Phys. **7**, 626 (2011).
[11] P. Wadley *et al.*, Science **351**, 587 (2016).
[12] V. Baltz, A. Manchon, M. Tsoi, T. Moriyama, T. Ono, and Y. Tserkovnyak, Rev. Mod. Phys. **90**, 015005 (2018).
[13] M. Binder, A. Weber, O. Mosendz, G. Woltersdorf, M. Izquierdo, I. Neudecker, J. R. Dahn, T. D. Hatchard, J.-U. Thiele, C. H. Back, and M. R. Scheinfein, Phys. Rev. B **74**, 134404 (2006).
[14] C. D. Stanciu, A. V. Kimel, F. Hansteen, A. Tsukamoto, A. Itoh, A. Kirilyuk, and T. Rasing, Phys. Rev. B **73**, 220402(R) (2006).
[15] V. V. Yurlov, K. A. Zvezdin, G. A. Kichin, M. D. Davydova, A. E. Tseplina, N. T. Hai, J.-C. Wu, S.-Z. Ciou, Y.-R. Chiou, L.-X. Ye, T.-H. Wu, R. C. Bhatt, and A. K. Zvezdin, Appl. Phys. Lett. **116**, 222401 (2020).
[16] M. D. Davydova, K. A. Zvezdin, J. Becker, A. V. Kimel, and A. K. Zvezdin, Phys. Rev. B **100**, 064409 (2019).
[17] M. D. Davydova, P. N. Skirdkov, K. A. Zvezdin, J.-C. Wu, S.-Z. Ciou, Y.-R. Chiou, L.-X. Ye, T.-H. Wu, R. C. Bhatt, A. V. Kimel, and A. K. Zvezdin, Phys. Rev. Appl. **13**, 034053 (2020).
[18] J. Han, A. Richardella, S. A. Siddiqui, J. Finley, N. Samarth, and L. Liu, Phys. Rev. Lett. **119**, 077702 (2017).
[19] N. Roschewsky, T. Matsumura, S. Cheema, F. Hellman, T. Kato, S. Iwata, and S. Salahuddin, Appl. Phys. Lett. **109**, 112403 (2016).
[20] R. Mishra, J. Yu, X. Qiu, M. Motapothula, T. Venkatesan, and H. Yang, Phys. Rev. Lett. **118**, 167201 (2017).
[21] J. Finley and L. Liu, Phys. Rev. Appl. **6**, 054001 (2016).
[22] Y. Yang, B. W. Richard, G. Jon, L. Charles-Henri, S. Sayeef, and J. Bokor, Sci. Adv. **3**, e1603117 (2017).
[23] F. Schlickeiser, U. Atxitia, S. Wienholdt, D. Hinzke, O. Chubykalo-Fesenko, and U. Nowak, Phys. Rev. B **86**, 214416 (2012).

[24] T. Kato, K. Nakazawa, R. Komiya, N. Nishizawa, S. Tsunashima, and S. Iwata, IEEE Trans. Magn. **44**, 3380 (2008).
[25] K.-J. Kim, S. K. Kim, Y. Hirata, S.-H. Oh, T. Tono, D.-H. Kim, T. Okuno, W. S. Ham, S. Kim, G. Go, Y. Tserkovnyak, A. Tsukamoto, T. Moriyama, K.-J. Lee, and T. Ono, Nat. Mater. **16**, 1187 (2017).
[26] S. A. Siddiqui, J. Han, J. T. Finley, C. A. Ross, and L. Liu, Phys. Rev. Lett. **121**, 057701 (2018).
[27] S.-H. Oh, S. K. Kim, D.-K. Lee, G. Go, K.-J. Kim, T. Ono, Y. Tserkovnyak, and K.-J. Lee, Phys. Rev. B **96**, 100407(R) (2017).
[28] E. Martínez, V. Raposo, and Ó. Alejos, J. Magn. Magn. Mater. **491**, 165545 (2019).
[29] B. A. Ivanov, E. G. Galkina, V. E. Kireev, N. E. Kulagin, R. V. Ovcharov, and R. S. Khymyn, Low Temp. Phys. **46**, 841 (2020).
[30] M. D. Davydova, K. A. Zvezdin, A. V. Kimel, and A. K. Zvezdin, J. Phys.: Condens. Matter **32**, 01LT01 (2019).
[31] A. P. Malozemoff and J. C. Slonczewski, *Magnetic Domain Walls in Bubble Materials*, Advances in Materials and Device Research, Vol. 1 (Academic Press, Cambridge, MA, 2016).
[32] See Supplemental Material at http://link.aps.org/supplemental/10.1103/PhysRevB.103.134442 for analytical details.
[33] A. K. Zvezdin, Sov. JETP Lett. **29**, 553 (1979).
[34] I. L. Kindiak, P. N. Skirdkov, K. A. Tikhomirova, K. A. Zvezdin, E. G. Ekomasov, and A. K. Zvezdin, Phys. Rev. B **103**, 024442 (2021).
[35] A. Zvezdin, Z. Gareeva, and K. Zvezdin, J. Magn. Magn. Mater. **509**, 166876 (2020).
[36] N. Awari, S. Kovalev, C. Fowley, K. Rode, R. A. Gallardo, Y.-C. Lau, D. Betto, N. Thiyagarajah, B. Green, O. Yildirim, J. Lindner, J. Fassbender, J. M. D. Coey, A. M. Deac, and M. Gensch, Appl. Phys. Lett. **109**, 032403 (2016).
[37] T. Shiino, S.-H. Oh, P. M. Haney, S.-W. Lee, G. Go, B.-G. Park, and K.-J. Lee, Phys. Rev. Lett. **117**, 087203 (2016).
[38] C.-F. Pai, M.-H. Nguyen, C. Belvin, L. H. Vilela-Leão, D. Ralph, and R. Buhrman, Appl. Phys. Lett. **104**, 082407 (2014).
[39] J. Sinova, S. O. Valenzuela, J. Wunderlich, C. H. Back, and T. Jungwirth, Rev. Mod. Phys. **87**, 1213 (2015).
[40] A. Mellnik, J. Lee, A. Richardella, J. Grab, P. Mintun, M. Fischer, A. Vaezi, A. Manchon, E.-A. Kim, N. Samarth, and D. Ralph, Nature (London) **511**, 449 (2014).
[41] V. Puliafito, R. Khymyn, M. Carpentieri, B. Azzerboni, V. Tiberkevich, A. Slavin, and G. Finocchio, Phys. Rev. B **99**, 024405 (2019).
[42] T. Okuno, D.-H. Kim, S.-H. Oh, S. K. Kim, Y. Hirata, T. Nishimura, W. S. Ham, Y. Futakawa, H. Yoshikawa, A. Tsukamoto, Y. Tserkovnyak, Y. Shiota, T. Moriyama, K.-J. Kim, K.-J. Lee, and T. Ono, Nat. Electron. **2**, 389 (2019).